

# Probing the Concept of Statistical Independence of Intermediate-Mass Fragment Production in Heavy-Ion Collisions

W. Skulski,\* J. Tőke, and W. U. Schröder

Dept. of Chemistry and NSRL, University of Rochester, Rochester, New York 14627

It is studied to what extent the characteristics of multi-IMF (intermediate-mass fragments) events can be derived from the properties of the observed single-IMF transverse-energy spectra. It is found that the spectra of total transverse IMF energy ( $E_t$ ) in multi-IMF events are well represented by “synthetic” spectra obtained by a multiple folding of the single-IMF transverse energy spectrum. Further, it is shown that, using the experimental IMF multiplicity distribution in the folding procedure, it is possible to reproduce the observed trends in the IMF multiplicity distributions for fixed values of the total transverse energy  $E_t$ . Accordingly, the “synthetic” multiplicity distributions show a binomial reducibility and an Arrhenius-like scaling similar to that reported in the recent literature. Consistent with the concept of statistical independence of multiple IMF production, similar results are obtained when the above folding-type synthesis is replaced with one based on mixing of events with different IMF multiplicities. For statistically independent IMF emission, the observed binomial reducibility and Arrhenius-like scaling are shown to be merely reflections of the shape of the single-IMF transverse-energy spectrum. Hence, a valid interpretation of these IMF distributions in terms of a particular production scenario has to explain independently the observed shape of the single-IMF  $E_t$  spectrum.

(PACS 25.70Lm, 24.10.Pa, 25.70.Mn, 25.70.Pq)

## 1. Introduction

Recently, in several studies<sup>1,2</sup> of heavy-ion-induced nuclear multifragmentation it was concluded that certain characteristics of the intermediate-mass fragment (IMF) data are suggestive of statistical independence of multiple IMF production.<sup>2</sup> Concepts of a binomial or a Poissonian reducibility<sup>1</sup> have been suggested to express the particular observed independence in mathematical terms. The concept of statistical independence or reducibility presumes that certain characteristics of multi-IMF events are reflections of the single-IMF production process. For example, the concept of a binomial reducibility<sup>1</sup> presumes that the probability of multiple IMF production is a reflection of the single-IMF production probability - the two quantities of interest being connected via the expression for a binomial distribution:

$$P_n^m(p) = \frac{m!}{n!(m-n)!} p^n (1-p)^{m-n}, \quad (1.1)$$

where  $P_n^m(p)$  is the multiple-IMF production probability and the parameters  $m$  and  $p$  are the number of (binomial) tries and the probability for success in any of these trials, respectively.

Although so far, no theoretical model has been proposed that would explain a binomial reducibility, one would reasonably expect that a successful model would at the same time link other characteristics of multi-IMF events to the characteristics of single-IMF production. With these expectations in mind, the present paper investigates, to what extent the empirical systematic of multiple IMF production can be derived from empirical characteristics of single-IMF production and, specifically, from the single-IMF transverse-energy spectrum. It is assumed in this study that the hypothesis of an independent IMF production holds and that, accordingly, the total transverse-energy spectra of multiple IMFs can be synthesized from the transverse-energy spectrum of a single IMF. Section 2 presents such a synthetic procedure, based on multiple folding of a schematic single-IMF spectrum. Section 3 discusses results obtained when empirical single-IMF spectra are substituted for the schematic distributions used in Section 2, and Section 4 discusses effects of an inclusion of transverse energies of light charged particles in the definition of the total transverse energy. An alternative synthesis method based on fragment swapping across different events of different IMF multiplicity is discussed in Section 5. Section 6 summarizes the findings of the present study.

## 2. Synthesis of Multi-Fragment $E_t$ distributions

In the following, the total transverse energy of charged reaction products is defined as

$$E_t = \sum_{i=1}^{mult} E_i \sin^2(\Theta_i), \quad (2.1)$$

where the summation extends over all particles with atomic numbers  $1 \leq Z \leq 20$ . In the present section, only IMFs with  $3 \leq Z \leq 20$  are included in the definition of  $E_t$ . Effects of

an inclusion of light charged particles are discussed further below, in Section 4. The following empirical characteristics of multi-IMF events represent the rationale behind the synthesis procedure presented in this section:

1. The  $E_t$  distributions of individual IMFs are approximately exponential, with inverse logarithmic-slope parameters  $T$  of the order of 30 to 50 MeV.<sup>2-5</sup> As an example, the experimental transverse-energy spectrum is shown in Fig. 1, for single IMFs from the Bi+Xe reaction<sup>2</sup> at  $E/A = 28$  MeV. Since  $E_t$  is an angle-integrated quantity, the corresponding spectrum may differ from a Maxwell-Boltzmann shape. Superimposed on the data are an exponential distribution with  $T = 50$  MeV (dotted line) and a two-parameter Gaussian fit (solid line) to the spectrum. While the exponential function deviates from the experimental spectrum both at high and low values of  $E_t$ , it simplifies the following demonstration of qualitative features of total IMF  $E_t$  spectra.

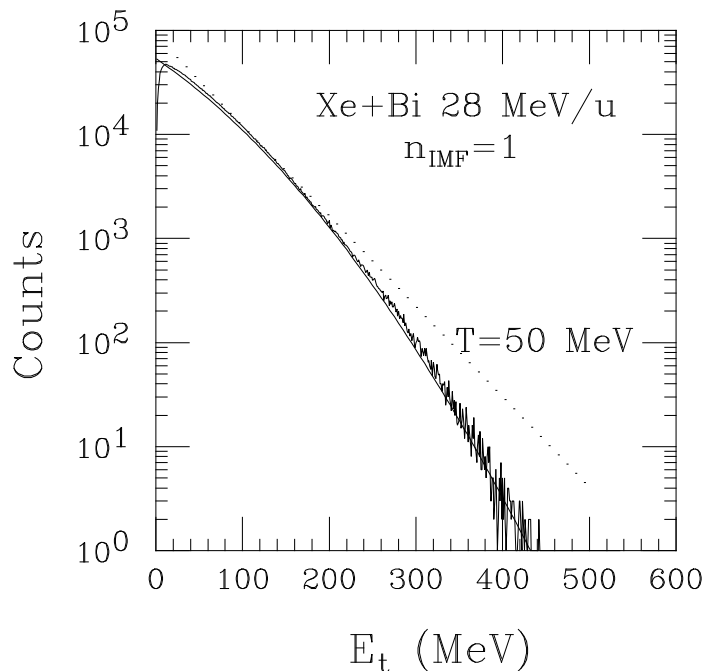


Fig. 1. Intermediate-mass fragment transverse-energy spectrum of single-IMF events. The dotted line is an exponential distribution,  $\exp(-E_t/T)$ , used as a first-order approximation of single-IMF spectra in Eq. 2.5. The spectrum itself was used as a model distribution  $\omega(e)$  for a numerical evaluation of the integrals (2.4) and (4.1) with a Monte Carlo method.

2. To a good approximation,  $E_t$  spectra of individual IMFs are independent of the IMF coincidence fold (multiplicity)  $n$ .<sup>2-5</sup> Although discernible, the dependence on  $n$  is weak.
3. In addition to IMFs, one also observes light charged particles (LCPs), which greatly outnumber IMFs, for every  $n$ . Even for  $n = 0$ , the average multiplicity of LCPs is of

the order of 10 and, hence, quite significant.

4. At low bombarding energies, e.g., for  $E/A \approx 30$  MeV, the IMF contribution can dominate the total transverse energy  $E_t$ , for all but the lowest multiplicities  $n$ .<sup>2,6,7</sup> For larger bombarding energies, the relative IMF contribution decreases but remains always significant.

Assuming a statistically independent IMF production, the probability distribution  $\Omega_n(e_1, \dots, e_n)$  for events with IMF multiplicity  $n$  can be expressed in the form of a product of  $n$  individual single-IMF distributions  $\omega_i(e_i)$

$$\Omega_n(e_1, \dots, e_n) = \prod_{i=1}^n \omega_i(e_i) \approx \prod_{i=1}^n \omega(e_i). \quad (2.2)$$

In Eq. 2.2, as in the following discussion, single-particle variables will be denoted by lower-case characters, while upper-case characters indicate multi-particle variables or distributions. For example, the symbol  $\Omega$  will be used to denote multi-particle probability distributions, while the symbol  $\omega$  indicates the corresponding single-particle distribution. Similarly, the variable  $e_i$  denotes the contribution of particle number  $i$  to the total (multi-particle) transverse energy  $E_t$ . While the first part of Eq. 2.2 represents the statistical independence, the second expresses the equality of all individual energy distributions.

Given the above form (2.2) of  $\Omega_n(e_1, \dots, e_n)$ , the distribution  $\tilde{\Omega}_n(E_t) = \tilde{\Omega}_n(e_1 + \dots + e_n)$  of the total transverse energy can be expressed as

$$\tilde{\Omega}_n(E_t) = \int dt_1 \cdots \int dt_{n-1} \Omega_n(t_1, \dots, t_n) \cdot \delta(E_t - t_1 - \dots - t_n), \quad (2.3)$$

where the integration is carried out over a hyperplane of a constant  $E_t$ , as enforced by the  $\delta$  function. Equation 2.3 can be further simplified to:

$$\tilde{\Omega}_n(E_t) = \int_0^{E_t} \omega(E_t - t_1) dt_1 \int_0^{t_1} \omega(t_1 - t_2) dt_2 \cdots \int_0^{t_{n-2}} \omega(t_{n-2} - t_{n-1}) \omega(t_{n-1}) dt_{n-1} \quad (2.4)$$

In the general case of an arbitrary individual single-particle distribution  $\omega$ , the integration in Eq. 2.4 can be performed numerically, at least for reasonably low IMF multiplicities. When a simple exponential function is taken to approximate  $\omega$ , this integral can be evaluated analytically for arbitrarily large IMF multiplicities:

$$\omega(e_i) = \beta \cdot \exp(-\beta \cdot e_i) \quad (2.5)$$

$$\tilde{\Omega}_n(E_t) = \beta \cdot \frac{1}{(n-1)!} \cdot (\beta E_t)^{n-1} \cdot \exp(-\beta \cdot E_t) \quad (2.6)$$

In principle, the inverse slope parameter  $\beta = 1/T$  could depend on the IMF multiplicity  $n$ , but the experimental dependence on  $n$  is known to be weak.<sup>3-5</sup> According to Eq. 2.6,

to the extent that the single-IMF transverse-energy spectra can be approximated by exponentials, the distribution of the composite observable  $E_t$  is of Poissonian form for each IMF coincidence order  $n$ .

In order to calculate quantitatively the two-dimensional joint probability distribution  $P(n, E_t)$  for a given reaction, one should combine the one-dimensional  $E_t$  distributions (2.6) for given  $n$ -values with the IMF multiplicity distribution  $y_n$ , measured for this reaction, i.e.,

$$P(n, E_t) = y_n \cdot \tilde{\Omega}_n(E_t) \quad (2.7)$$

Typical experimental  $y_n$  distributions are depicted in Fig. 2. For the experimental data discussed here, they can be approximated well by Gaussians,  $y_n \propto \exp(-(n-1)^2/2 \cdot \sigma^2)$  (solid line in the figure).

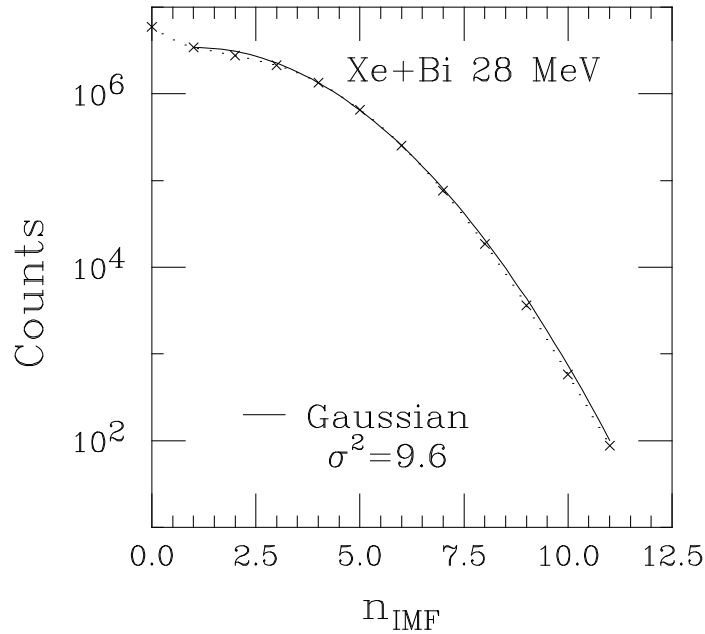


Fig. 2. Intermediate-mass fragment yield distribution of  $n$ -fold IMF events, for  $n = 0, 1, 2, \dots$ . The solid line is a Gaussian distribution,  $y_n \propto \exp[-(n-1)^2/2 \cdot \sigma^2]$ . This yield distribution was used for a numerical evaluation of the integrals (2.4) and (4.1) with a Monte Carlo method.

The joint distribution in Eq. 2.7 allows one to synthesize conditional IMF multiplicity distributions, gated with different values of  $E_t$ , and to calculate the binomial parameters  $m$  and  $p$  for these distributions for further analysis along the lines adopted in a series of recent papers.<sup>1</sup> Specifically, one calculates

$$\bar{n} = \sum_{i=1}^N i \cdot P(i, E_t) / \sum_{i=1}^N P(i, E_t), \quad (2.8)$$

$$\sigma_n^2 = \sum_{i=1}^N (i - \bar{n})^2 \cdot P(i, E_t) / \sum_{i=1}^N P(i, E_t), \quad (2.9)$$

$$m = \bar{n}/p, \tag{2.10}$$

$$p = 1 - \sigma_n^2/\bar{n}. \tag{2.11}$$

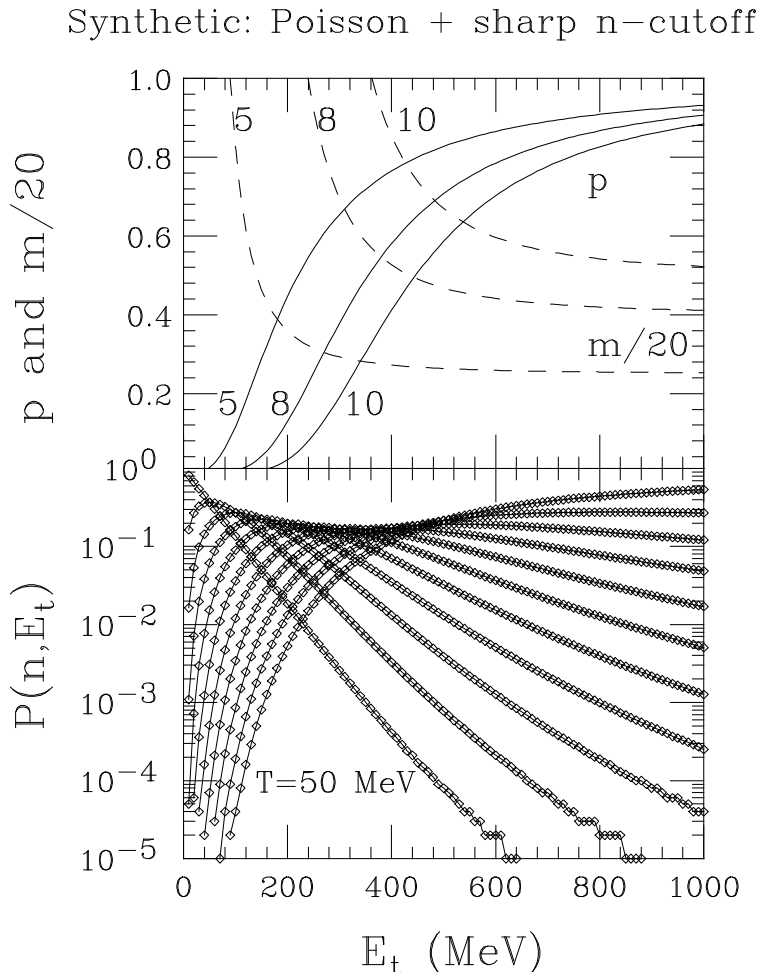


Fig. 3. Lower panel: The distributions (2.6) are plotted up to the order of  $N = 11$ . Note the qualitative similarity of the distributions (2.6) and the  $E_t$  distributions due to multifragmentation, plotted in the subsequent figures. Upper panel: The values of parameters  $p$  and  $m$  calculated with equations (2.11) and (2.10) and distributions (2.6), with sharp-cutoff weights  $y_n = 1$ , for  $n$  up to  $N$ , and  $y_n = 0$  for  $n > N$ . Three example values of  $N = 5, 8, 10$  are indicated in the figure. Note the severity of the truncation effect, which causes the calculated  $p$  and  $m$  to deviate from their limiting values, zero and infinity, respectively. The limits are reached only for  $N$  approaching infinity.

It is the use of the constrained empirical distribution  $y_n$  that leads to a reduction of the variances of the conditional multiplicity distributions below the Poissonian limit of  $\bar{n} = \sigma_n^2$  and, hence, ensures positive values for the parameters  $m$  and  $p$ . This is illustrated in Fig. 3, where a schematic sharp-cutoff distribution of  $y_n$  serves to demonstrate the importance of

truncation. Note the large magnitude of the truncation effect, which causes the calculated parameters  $p$  and  $m$  to deviate from their limiting values, zero and infinity, respectively. These limits are reached only when the number of folds approaches infinity. Significant values for both  $p$  and  $m$  have been generated within the physically relevant range of  $E_t$  by restricting the number of folds to  $\approx 10$ , i.e., a number of coincidence folds typically measured in an experiment.

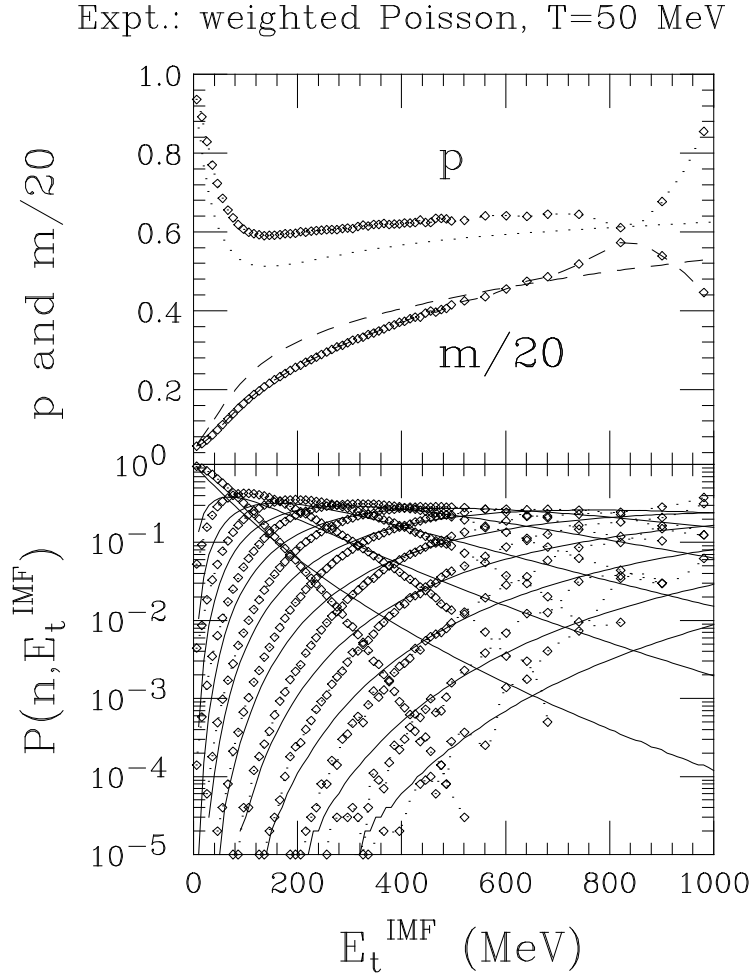


Fig. 4. Lower panel: The  $E_t$  distributions (2.7) weighted with the experimental IMF yields  $y_n$  are compared with experimental IMF-only transverse-energy distributions. The upper part of the figure shows the respective  $p$  and  $m$  parameters as calculated with Eqs. (2.11) and (2.10), respectively.

The synthetic distributions are compared in Fig. 4 with experimental IMF transverse-energy distributions. In the calculations, the IMF yields  $y_n$  were taken from experiment.<sup>8</sup> The inverse slope parameter  $\beta^{-1} = 50$  MeV of the IMF spectra was adjusted to approximately match the singles ( $n = 1$ ) spectrum up to about 200 MeV (see Fig. 1). As seen in this figure, already a synthesis using an exponential singles spectrum reproduces qualitatively the gross features of the experimental  $E_t$  distributions. The lack of a quantitative

agreement with experimental data is not surprising, since the used schematic exponential single-particle distribution (2.5) is only a very crude approximation of the actual single-particle spectrum. As seen in Fig. 1, the tail of the exponential function does not match the  $n = 1$  spectrum for  $E_t > 200$  MeV. Nevertheless, the overall features of the experimental  $E_t$  distributions are reproduced qualitatively by those calculated with Eq. 2.7.

The upper part of Fig. 4 presents a comparison between the parameters  $p$  and  $m$ , extracted from experimental data, with the ones calculated from Eqs. 2.8 and 2.9, using the distributions (2.7) displayed in Fig. 2. The predicted values of  $p$  and  $m$  match the experiment remarkably well, even though the calculated  $E_t$  distributions in the lower panel deviate from the experimental ones. This points towards the need for a better description of experimental single-fragment  $E_t$  distributions  $\omega(e)$ . More realistic shapes of these single-particle distributions will be considered next.

### 3. Synthesis with Realistic Single-IMF Distributions

A more realistic rendering of the shape of the single-IMF distribution than achieved by an exponential is provided by a two-parameter Gaussian fit of the kind depicted by the solid line in Fig. 1. Such a Gaussian spectrum was used in a numerical evaluation of the integrals (2.4), employing a Monte-Carlo sampling method results of which are displayed in Fig. 5. As seen in Fig. 5, a remarkable quantitative agreement with experimental data is achieved. This time, also the parameters  $p$  and  $m$  have been reproduced. It is worth emphasizing, that only four parameters, two shape parameters of the single-particle spectrum (cf. Fig. 1) and two parameters describing the IMF yield distributions (cf. Fig. 2)) are sufficient to reproduce the shapes of the multi-IMF  $E_t$  distributions, and the  $E_t$ -dependencies of the parameters  $p$  and  $m$ .

### 4. The Role of LCP Contributions

In order to better represent the experimental situation, the contribution by light charged particles to the total kinetic energy has to be considered. This can be achieved easily by extending the concept of a statistically independent fragment production to the LCP emission. In this case,

$$\tilde{\Omega}_n(E_t) = \tilde{\Omega}(e_0 + e_{1+}, \dots, +e_n) = \int_0^{E_t} \omega_0(E_t - t_0) dt_0 \int_0^{t_0} \omega(t_0 - t_1) dt_1 \dots \quad (4.1)$$

The index 0 now denotes the LCP contribution to the total  $E_t$ . Since there are many LCPs contributing independently (even for the case of no IMFs,  $n = 0$ ), according to the Central Limit Theorem, the contribution of all LCP's, taken together, is approximately a Gaussian

$$\omega_0(e_0) \propto \exp [-(e_0 - \bar{e}_0)^2 / 2\sigma_0^2], \quad (4.2)$$



where the parameters  $\bar{e}_0$  and  $\sigma_0$  may depend on the IMF multiplicity  $n$ .

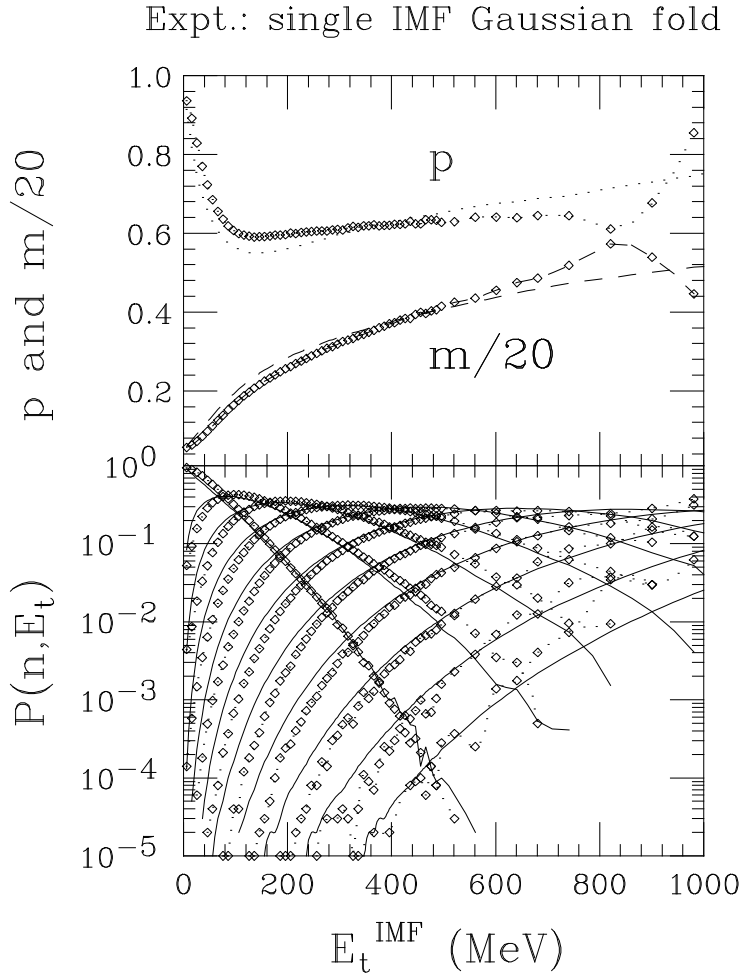


Fig. 5. Lower panel: IMF transverse- energy distributions (solid lines), predicted by folding a Gaussian form of the  $n = 1$  IMF distribution multiple times with itself (without the LCP contribution), according to formula (2.4). The resulting  $E_t$  spectra were weighted with the Gaussian IMF yields  $y_n$  from Fig. 2. The symbols connected with dotted lines represent experimental data. Upper panel:  $p$  and  $m$  parameters extracted from the experimental data (symbols connected with lines), compared with the ones extracted from the set of folded  $E_t$  distributions.

Wieloch et. al.<sup>4,5</sup> have considered the particular parameterization of  $\bar{e}_0 \propto n$  and  $\sigma_0 = \text{const}$ . The present paper employs values of  $\bar{e}_0$  and  $\sigma_0$  taken from experiment,<sup>8</sup> namely  $\bar{e}_0 \propto n$  for  $n = 0, 1, 2$  and  $\bar{e}_0 \approx \text{const}$  for  $n \geq 2$ . With this choice of parameter values  $\bar{e}_0$  and  $\sigma_0$ , the integral (4.1) was evaluated numerically in the same way as before. The results are displayed in Fig. 6, showing satisfactory agreement with experimental data. The parameters  $p$  and  $m$  are also rather well reproduced by the calculation, except for the deviations from experimental data at  $E_t < 100$  MeV. The deviations are attributed to an imperfect representation of LCP spectra by Gaussians, and in particular to the intense

contributions of peripheral events to the LCP spectra at low  $E_t$ . It should be noted, that low- $E_t$  data are usually considered less important in the context of multifragmentation.

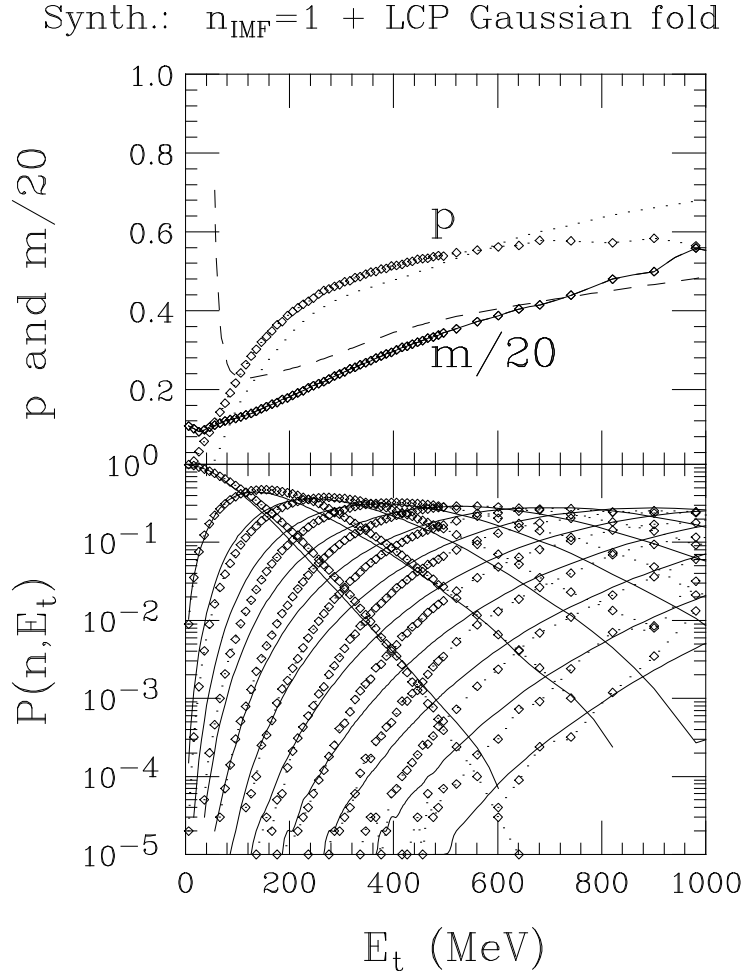


Fig. 6. Lower panel: IMF transverse- energy distributions (solid lines), predicted by folding a Gaussian approximation to the  $E_t$  distribution for  $n = 1$  multiple times with itself and with the LCP contributions, according to formula (4.1). The resulting  $E_t$  spectra were weighted with the yields  $y_n$  from Fig. 3. The symbols connected with dotted lines represent experimental data. Upper panel: Experimental  $p$  and  $m$  parameters are compared with those predicted by folding.

## 5. Mixed-event calculations

As an alternative approach to synthesizing multi-IMF events, the experimental data<sup>8</sup> have been subjected to “event mixing”, a procedure where both IMFs and LCPs are randomly exchanged between different events. For every event, the number of LCPs,  $n_{LCP}$ , and the number of IMFs,  $n$ , were preserved, but not the identities of these particles. Both IMFs and LCPs were swapped among events of all multiplicities (regarded as a common “fragment

pool”), in order to ensure a complete “loss of memory” in the synthetic mixed–event data set.

The above random particle exchange between events ensured that multi-particle correlations were erased from experimental data, while preserving approximately the shape of the single-particle distributions. In this fashion, a statistical independence among particles was strictly imposed on experimental data, even if some degree of multi-particle correlations had been present in the original data set. This procedure ensured that the assumptions underlying Eq. 4.1 were strictly fulfilled by the data. It should be stressed, that event mixing does not represent any additional assumption brought into the problem. Rather, it is a convenient way to evaluate the integral (4.1), where all single–particle probability distributions were sampled directly from the experimental data, without recourse to a particular parameterization.

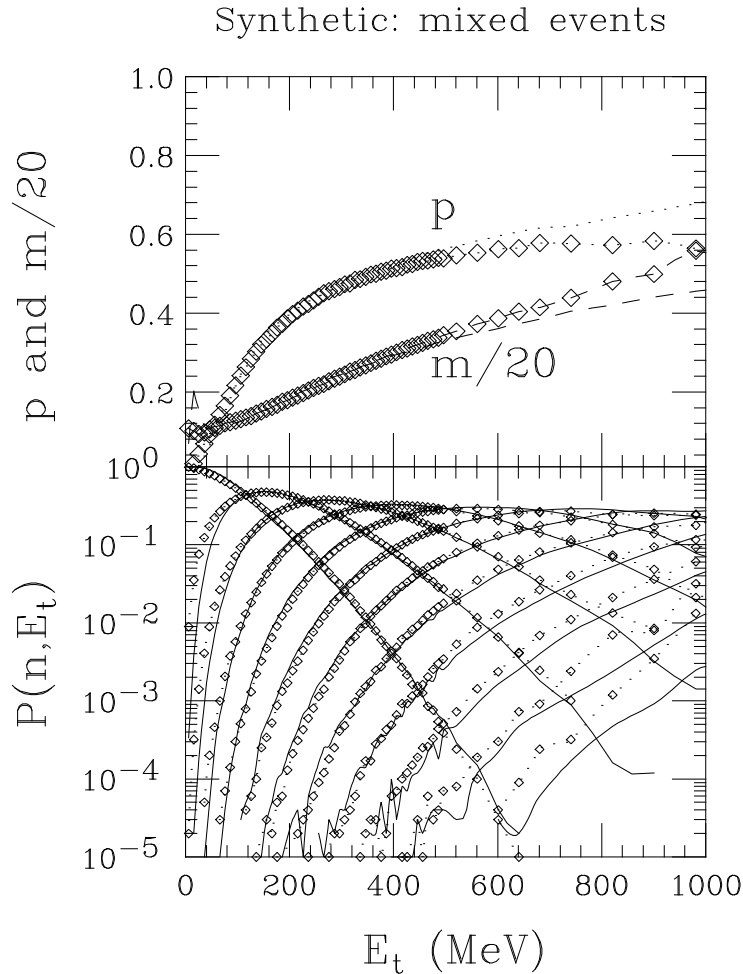


Fig. 7. Transverse-energy distributions (lower panel) and  $p$  and  $m$  parameters (symbols with dotted line in upper panel) extracted from the experimental data set and from the same set, but subjected to random particle swapping (solid lines).

Subsequently, the synthetic events were subjected to the same analysis procedure as the

original data. The results of this mixed-event analysis are compared with the original data in Figs. 7 and 8. Very good agreement between both sets of results is observed from these figures, both with regard to the  $E_t$  distributions and the extracted parameters  $p$  and  $m$ . This result confirms again that the concept of a statistically independent IMF production is a valid one.

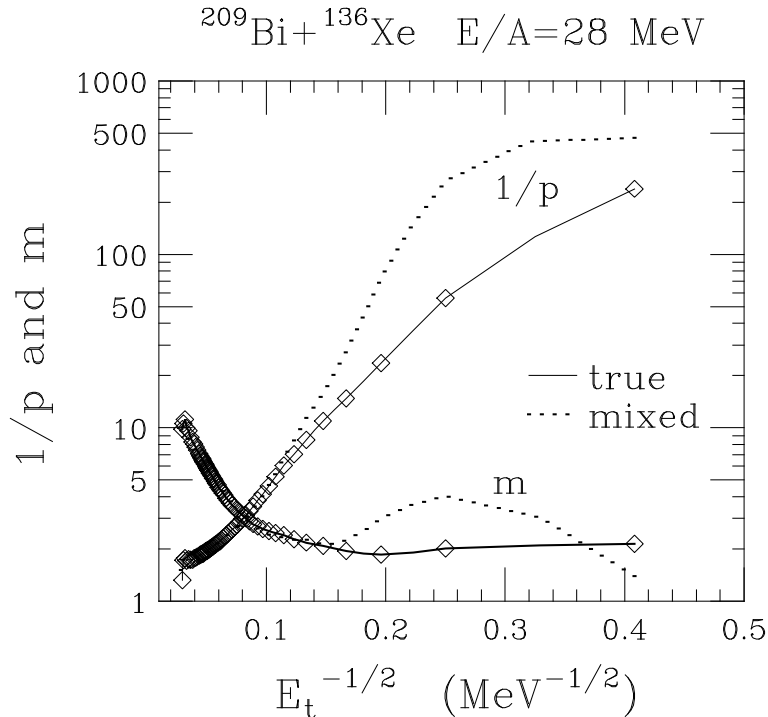


Fig. 8. The  $p$  and  $m$  parameters extracted from the experimental data set (symbols connected with solid line) and from the same set subjected to random particle swapping (dotted lines), plotted in an Arrhenius-like representation as functions of  $E_t^{-1/2}$ .

## 6. Summary

Accepting the validity of the findings of earlier papers<sup>1,2</sup> regarding the statistical independence, or reducibility, of multiple intermediate-mass fragment production, one finds that important characteristics of multi-IMF events can be derived already from the experimental shapes of single-IMF transverse energy distributions. The characteristics of the synthetic events generated from these distributions show remarkable resemblance to those of the experimental multi-IMF events. The latter characteristics include the binomial reducibility and an Arrhenius-like scaling discovered in recent studies of nuclear multifragmentation.<sup>1</sup>

Although the findings of the present study do not directly favor one IMF production scenario over another, they do so indirectly. They draw attention to the crucial importance of an understanding of the shapes of the single-IMF  $E_t$  distributions. In the present analysis, the apparent binomial reducibility and the apparent Arrhenius-like scaling are secondary

phenomena, both reflecting the “input” shape of the elementary  $E_t$  distribution. Hence, a valid interpretation of the significance of such reducibility and scaling in terms of a particular IMF production scenario requires an independent explanation of the underlying single-IMF  $E_t$  distribution.

A purely thermal scenario, which could potentially justify Arrhenius-like correlations between emission probability and temperature of the system, makes quite definite predictions regarding the elementary  $E_t$  distributions, which should be very similar to those of the lighter particles emitted from the same sources. These predictions disagree with the experimental IMF spectra, which are significantly harder than the light-particle  $E_t$  spectra. This observation justifies some skepticism towards an interpretation<sup>1</sup> of Arrhenius-like plots in terms of thermal scaling.

## 7. Acknowledgements

The Bi+Xe experiment at  $E/A = 28$  MeV was conducted in collaboration with S.P. Baldwin, B. M. Quednau, L.G. Sobotka, J. Barreto, R. J. Charity, L. Gallamore, D.G. Sarantites, D. W. Stracener, R. T. de Souza, and B. Lott. Their contribution is highly appreciated.

This work was supported by the U. S. Department of Energy Grant No. DE-FG02-88ER40414.

## 8. References

- 
- \*. Present address: X-Ray Instrumentation Associates, 2513 Charleston Road, Suite 207, Mountain View, CA 94043, USA
  1. L.G. Moretto, R. Ghetti, L. Phair, K. Tso, G.J. Wozniak, Phys. Rep. 287, 249 (1997), and references therein.
  2. J. Töke, et al., Phys. Rev. Lett. **77**, 3514 (1996).
  3. J. Töke et. al., *Advances in Nuclear Dynamics 2*, Proceedings of 12th Winter Workshop on Nuclear Dynamics, February 3-10, 1996, Snowbird, Utah. Edited by W. Bauer and G.D. Westfall, Plenum Press 1996.
  4. A. Wieloch et. al., Z.Phys. A359, 345 (1997).
  5. A. Wieloch et. al., Phys. Lett. B**432**, 29 (1998).
  6. W. Skulski et. al., Report DOE/ER/40414-8, page 75 and 86 (1995).

7. L.Phair, private communication.
8. J. Tőke et. al., Phys. Rev. C**56**, R1683 (1997).